

Emission cross sections for electron-impact excitation of zinc atoms

S. A. Napier,¹ D. Cvejanović,^{1,2} J. F. Williams,^{1,2,*} L. Pravica,^{1,2} D. Fursa,³ I. Bray,³ O. Zatsarinny,⁴ and K. Bartschat⁴¹Centre for Atomic Molecular and Surface Physics, School of Physics, University of Western Australia, Perth 6009, Australia²ARC Centre for Antimatter-Matter Studies, School of Physics, University of Western Australia, Perth 6009, Australia³ARC Centre for Antimatter-Matter Studies, School of Science, Curtin University, Perth 6845, Australia⁴Department of Physics and Astronomy, Drake University, Des Moines, Iowa 50311, USA

(Received 1 February 2009; published 1 April 2009)

Experimental and theoretical studies of the electron-impact excitation of the $(4s4p) \ ^1\text{P}_1$, $(4s5s) \ ^3\text{S}_1$, and $(4s4d) \ ^1\text{D}$ states of zinc atoms are reported. Relative emission cross sections were measured from the excitation thresholds to 50 eV incident energy. Theoretical angle-integrated and emission cross sections were obtained using the convergent close-coupling and B -spline R -matrix methods. The measured data were normalized to theory and are discussed in terms of electron spin and correlation effects. The studies highlight the significance of both channel coupling to the continuum and the inner $3d$ -shell electrons.

DOI: 10.1103/PhysRevA.79.042702

PACS number(s): 34.80.Dp

I. INTRODUCTION

This joint experimental and theoretical investigation of electron-impact excitation of zinc atoms follows our previous experimental and theoretical studies [1–7]. The work concerns angle-integrated cross sections (ICSS) for direct excitation and emission cross sections (ECSs) for selected states from their excitation threshold to 50 eV. The zinc target, the particular excited states, and the energy range were selected to encompass observable electron correlation effects, which could be investigated by leading-edge experimental and theoretical approaches. The studies also aim to look at the effects of spin-dependent interactions [4] in electron-impact excitation collisions. The data have applications in the development of new and improved light sources, which at the same time are environmentally friendly [8].

Recent advances concerning the interaction of complex many-electron atoms with both electrons and photons have elucidated the role and extent of electron correlations, channel coupling, and relativistic effects, as well as appropriate ways for their theoretical description. Electron-impact coherence parameters or Stokes parameters, obtained from both electron-photon coincidence experiments and superelastic scattering setups, generally provide detailed tests of theoretical models. Unfortunately, such experiments have limitations due to either long data accumulation times (in coincidence experiments) or the inability to access a range of optically forbidden transitions and those for which no suitable lasers are available (in superelastic scattering). Interestingly, many of these angle-differential parameters are not particularly sensitive to relativistic effects [9] and thus are often reproduced well by sophisticated, although nonrelativistic theories—even for very heavy atoms [9,10]. Somewhat surprisingly, angle-integrated Stokes parameters measured after spin-polarized electron impact are occasionally more appropriate [11].

Theoretical approaches that assume an inert inner core successfully model many experimental data for quasi-one-

and quasi-two-electron atoms [12,13], but certainly not for all such atoms and not for all observables [14,15]. Consequently, we are continuing our studies of the zinc atom, where a wide range of many-electron effects is observed and has indicated significant advances [4] in elucidating the characteristics of the excitation process.

Recent experimental studies in zinc (see [6,7] and references therein) identified the presence and the effects of negative-ion resonances both below and above the ionization threshold. Above the ionization threshold, we studied temporary negative-ion resonance states, which are formed by the excitation of an inner $3d$ electron. Particular emphasis was put on electron correlations and spin-dependent effects. In this energy region, the decay of autoionizing states excited near their excitation threshold exhibits correlation effects, which have been observed to significantly affect the excitation of higher-lying states of zinc [7]. Here the postcollision interaction (PCI) between the scattered and the ejected electrons, both of which are relatively slow, includes a transfer of up to two units of angular momentum and has large effects on the excitation of the $n=4, 5, 6 \ ^3D_{1,2,3}$ states [7]. While negative-ion resonances have been described well in zinc by theory for electron-impact energies up to approximately 8 eV [1], there are no theoretical studies above the ionization threshold of either PCI effects or negative-ion resonances, although the classic Fano profile is evident.

There are only a few experimental and theoretical studies characterizing the excitation of zinc in terms of cross sections. Angle-differential and angle-integrated experimental and theoretical cross sections were reported recently for excitation of the $(4s4p) \ ^1P_1$ and $(4s5p) \ ^1P_1$ states by Fursa *et al.* [2]. Experimental values were reported for incident electron energies of 15, 20, 25, 40, and 60 eV for the $(4s4p) \ ^1P_1$ state and at 20, 25, and 40 eV for the $(4s5p) \ ^1P_1$ state. The nonrelativistic convergent close-coupling (CCC) method was used in the calculations and good agreement between theory and experiment was established. Similarly good agreement was found with the angle-differential cross section (DCS) for $^1S_0 \rightarrow ^1P_1$ excitations for small scattering angles reported by Panajotović *et al.* [16], but not with earlier 40 eV $(4s4p) \ ^1P_1$ DCS measurements of Williams and Bozinis [17].

*jfw@cyllene.uwa.edu.au

Angle-integrated cross sections were also measured by Shpenik *et al.*[18] for $(4s4p) \ ^3P_{0,1,2}$ (from threshold to 6.5 eV) and $(4s4p) \ ^1P_1$ (from threshold to 16 eV). On the theoretical side, angle-integrated cross sections were reported for excitation of the $(4s4p) \ ^{1,3}P_1$, $(4s4d) \ ^1D_2$, $(4s5s) \ ^{1,3}S$, $(4s5p) \ ^1P_1$, and $(3d^9 4s^2 4p) \ ^1P_1$ states by Zatsarinny and Bartschat [1] using the *B*-spline *R*-matrix (BSR) method, also in the non relativistic mode.

In this paper we report on the angle-integrated excitation cross sections and also emission cross sections for five excited states of zinc, namely, $(4s4p) \ ^{1,3}P_1$, $(4s5s) \ ^3S_1$, and $(4s4d) \ ^{1,3}D$. These include optically allowed, spin-forbidden, symmetry-forbidden, and both spin- and symmetry-forbidden excitations. The more complex excitations, for example, those forbidden by dipole selection rules, generally present the most demands on the theoretical modeling. Previous experimental studies indicate that the *3d*-core shell in zinc is not inert. Consequently, the *3d* electrons play a significant role in the scattering process, as soon as their excitation becomes energetically possible.

At the present time, there is no theory available for targets as complex as the Zn atom, which can be expected to reproduce all the experimental data for the transitions presented in this paper. As will be seen below, the CCC method can account for coupling to the ionization continuum, but is restricted to an inert core, i.e., *3d*¹⁰ in the present case, as well as the treatment of relativistic effects through the recoupling of nonrelativistic results. A full-relativistic version, however, has just been developed and successfully tested for quasi-one-electron targets such as Cs [19]. On the other hand, the BSR method can allow for coupling to open-core states and treat relativistic effects at the level of the Breit-Pauli [20] and even the Dirac-Coulomb [21,22] description, but the number of states required to couple to the target continuum in a converged way is beyond our currently available computer codes and computational resources. However, the comparison results from simplified CCC and BSR models, starting from approximately the same level of accuracy, with those from more sophisticated calculations that can be performed only by either one of the two methods, should give an indication about which of these effects are the most important for a particular transition. Finally, comparison with experiment allows for an assessment of the accuracy that can be obtained by the most sophisticated currently available theoretical methods.

II. EXPERIMENT

The experimental apparatus is the same as in our previous studies of negative-ion resonances in zinc [6,7]. It was used here, however, in a different way to satisfy the requirements for accurate cross-section measurements. Briefly, a beam of electrons with a current of ~300 nA and a full width at half maximum energy spread of 250 meV was crossed with a zinc vapor beam originating from a resistively heated molybdenum oven. The electron optics for the incident electron beam was optimized for constant current transmission, rather than energy resolution, by using a high-pass kinetic energy through a 127° electrostatic energy selector.

Decay photons were detected using an Electron Tubes 9863/350QB photomultiplier tube (PMT) positioned at an angle of 90° to the incident electron beam direction. The photon wavelength was selected by an interference filter, and the photon polarization was analyzed using a combination of a computer-controlled liquid-crystal variable retarder and a linear polarizer [23].

The incident beam current and the emitted photon count rates were recorded simultaneously, so that the photon count rate could be normalized to constant current. Background photons were recorded for each measurement and subtracted from the measured signal.

Other factors were approximately constant during individual scans, but varied between scans. For example, there was some difference in the oven flux between scans, as well as the lens or window transmission at different times because of zinc deposition. The data reported below were usually obtained from two scans across the energy range, normalized to each other, and then averaged to give the final values. The normalization factor was the ratio of the photon signal for each scan summed over all energies. The variation between individual scans was larger than that given by the usual counting statistics. The uncertainty in the experiment was quantified by calculating the percentage difference between the two scans at each data point before finding the average percentage difference across all data points for all states studied. This average percentage difference, and thus the estimated uncertainty of the present measurements, was 12%.

The photon count rate was adjusted for polarization of the detected radiation using the energy-dependent linear light polarization *P* in Eq. (1.2) of Percival and Seaton [24]. The adjusted intensity has the form

$$I = I(90^\circ) \left(1 - \frac{P}{3} \right), \quad (1)$$

where *I*(90°) denotes the photon intensity measured at 90° to the incident electron beam while *I* is the intensity integrated over all angles and hence proportional to the emission cross section.

The Stokes polarization parameter *P* appearing in Eq. (1) is determined by

$$P = \frac{I_{0^\circ} - I_{90^\circ}}{I_{0^\circ} + I_{90^\circ}}, \quad (2)$$

where *I*_{α°} is the intensity of photons passed through the linear polarizer with transmission axis at an angle α° to the direction of the incident electron beam. The polarimeter used in the present study limited the polarization analysis to visible wavelengths.

As mentioned above, measurements were performed for five excited states of zinc, namely, $(4s4p) \ ^{1,3}P_1$, $(4s4d) \ ^{1,3}D$, and $(4s5s) \ ^3S_1$ for decay radiation wavelengths of λ=307.6, 213.8, 481.0, 636.0, and 334.2 nm, respectively, from near threshold to 50 eV incident energy in 1 eV intervals. The typical data collection time was around 120 s per energy point. For the $(4s4d) \ ^1D_2$ state, the light polarization *P* was also measured, and the intensities were then corrected as indicated by Eq. (1) to obtain the emission cross section.

The interference filters and other details relevant for photon isolation and detection were discussed in our previous publications [6,7]. The measured intensities were normalized to theoretical CCC values at an appropriately chosen energy, namely, 40 eV for singlet and 30 eV for triplet states. These energies are well above the region where temporary negative-ion resonances and PCI effects associated with excitation of an inner $3d$ electron are important; both of which are not described by the CCC e -Zn scattering model. On the other hand, coupling to high-lying excited states and the ionization continuum is expected to be important at these energies. These effects are well described within the CCC method.

The energy calibration was performed by measuring the $\lambda=636.2$ nm photons from the decay of the $(4s4d) \ ^1D_2$ state in the vicinity of the excitation threshold and comparing with the BSR results for the angle-integrated cross section after convolution with the experimental energy resolution (see [6] for details.) With the present energy resolution, this calibration resulted in an uncertainty of 100 meV.

III. THEORETICAL APPROACHES

A. CCC method

We used the nonrelativistic formulation of the CCC method [25,26] to perform the e -Zn scattering calculations. The present application of the CCC method to e -Zn scattering differs only in minor details from the previous CCC calculations reported by [2]. However, for ease of comparison between the CCC and BSR methods, we briefly restate the most important details here.

The Zn atom is described by a model of two active electrons above a frozen Hartree-Fock $[\text{Ar}]3d^{10}$ core. The core orbitals are obtained via Zn^+ Hartree-Fock calculations. We then generate a set of one-electron orbitals via diagonalization of the Zn^+ frozen-core quasi-one-electron Hamiltonian in the basis of Sturmian (Laguerre) functions. A total of 42 Laguerre basis functions for each of the orbital angular momenta $l=0, 1, 2,$ and 3 with exponential fall-off parameters $\lambda_l=2.4, 2.2, 1.74,$ and $1.6,$ respectively, were employed. We retained 9, 8, 8, and 5 low-lying Zn^+ orbitals for $l=0, 1, 2, 3,$ respectively, which were then used in standard two-electron configuration-interaction (CI) calculations to produce a set of target states for the zinc atom. In order to account for electron-electron correlations with a sufficient accuracy, a set of two-electron configurations was chosen, in which one electron occupies either the $4s$ or $4p$ orbital while the other electron may occupy any other orbital.

In order to account approximately for core-valence correlations, we included both one-electron and two-electron polarization potentials [26]. The parameters of the one-electron polarization potential, namely, the static dipole polarizability of the Zn^{2+} ion, $\alpha_d=2.6,$ and the exponential cutoff, $\rho_l=1.38,$ were chosen to yield a good representation of the Zn^+ low-lying energy spectrum and were kept the same for all values of the orbital angular momentum $l.$ The parameters of the two-electron polarization potential, $\alpha_d=2.6,$ and the exponential cutoff, $\rho=2.18,$ were chosen to fit the ground-state energy and the optical oscillator strength for the

$(4s4p) \ ^1P_1 \rightarrow (4s^2) \ ^1S_0$ resonance transition close to their experimental values.

The CI calculations produced a total of 206 singlet and triplet states with total orbital angular momentum ranging from zero to four. This structure model leads to 29 negative-energy states (relative to the Zn^+ ground state) with the low-lying negative-energy states [up to $(4s6d) \ ^3D$] giving a good representation of the Zn bound spectrum. The remaining positive-energy states provide a square-integrable discretization of the target continuum and allow us to account for coupling to ionization channels in the scattering calculations. The set of Zn target states obtained in this way is then used to set up a multichannel expansion of the total wave function of the e -Zn collision system and to solve a system of Lippmann-Schwinger close-coupling equations for the T -matrix elements [25]. Finally, the scattering amplitudes and cross sections for the transitions of interest are obtained from the calculated T -matrix elements in a standard manner.

In addition to the CCC206 model described above, we performed several other calculations with different numbers of states in order to establish convergence of the presented cross sections. The CCC162 and CCC262 models were produced in the same way as the CCC206 model, but with smaller (larger) number of Zn^+ orbitals retained. The cross sections obtained with these three models proved to be sufficiently close. Hence mostly CCC206 results are presented below, with the exception of the $(4s4p) \ ^3P_1$ state, where the additional coupling makes a significant difference for some energies.

Finally, however, we performed calculations in a CC29 model, which couples only the 29 negative-energy states generated for the CCC206 model. Comparison of the CCC206 and CC29 model results allows us to estimate the effect of coupling to the ionization channels on the calculated cross sections.

B. BSR method

This method has been described in detail by Zatsarinny and Bartschat [1]. Hence we only summarize the most important aspects here. There are two essential differences to the CCC approach described above: (1) as an *all-electron code*, the BSR program [20] allows us to include the core-valence correlation *ab initio* by adding target configurations with an excited core and (2) due to the nature of the R -matrix method, which employs an expansion of the collision wave function in terms of a basis set in the “inner region,” where electron exchange and correlation effects are important, it is usually not possible to couple as many states as in the CCC approach. Furthermore, the range of projectile energies is limited by the size of the basis. As a result of these numerical aspects, the R -matrix method is generally very efficient when results for a large number of collision energies are required, e.g., in near-threshold resonance regions. On the other hand, the CCC approach, which directly solves the Lippmann-Schwinger equations for the transition matrix at a given energy, is expected to be more reliable for “intermediate” and also for “high” incident energies. For these energies, mostly above the ionization threshold, resonance effects are often

small (except when inner-shell excitation becomes significant), but coupling to the ionization continuum can become very important.

Specifically, we used the B -spline box-based close-coupling method [27] to generate the target states, including 67 B splines of order 8 to span the radial region from the origin to the R -matrix radius of $a=35a_0$. We started by generating the core orbitals from a Zn^{2+} Hartree-Fock calculation and then obtained valence $4s$, $4p$, $4d$, and $5s$ orbitals from a frozen-core calculation for Zn^+ . We then simulated the core-valence correlation by adding the $3d^9\bar{n}\ell\bar{n}\ell'$ configurations, where the bar indicates a correlated rather than a physical orbital. The different sets of correlated orbitals $\bar{n}\ell$ were optimized for each Zn^+ state separately. Since the mean radii for the $\bar{n}\ell$ orbitals lie between the mean radii of the core and the valence orbitals, this method allows us to incorporate the core-valence correlation with a relatively small number of configurations.

The core-valence correlated states of Zn^+ were used then as target states in B -spline bound-state close-coupling calculations to generate the low-lying states of atomic Zn. As described in [1], this scheme yields term-dependent, nonorthogonal orbital sets for each LS term. The number of physical states that we can generate in this method depends on the size a of the R -matrix box. With $a=35a_0$, we obtained a good description for all low-lying states of Zn up to $(4s6s)^1S$. Along with these physical states, we also generated a set of pseudostates for each symmetry, with the lowest states representing the remaining bound states and the others representing the continuum. The accuracy of the structure calculation can be assessed by the excitation energies and the oscillator strengths listed in Tables I and II of [1]. Note that the experimental energy splittings for the spectroscopic states were used in the subsequent scattering calculations. This allows for a direct comparison between experiment and theory.

The scattering calculations were carried out with the recently developed B -spline R -matrix code [20]. Once again, the distinctive feature of the method is the use of B splines as a universal basis to represent the scattering orbitals in the inner region of $r \leq a$. Hence, the R -matrix expansion in this region takes the form

$$\Psi_k^\Gamma(x_1, \dots, x_{N+1}) = \mathcal{A} \sum_{ij} \bar{\Phi}_i^\Gamma(x_1, \dots, x_N; \hat{\mathbf{r}}_{N+1} \sigma_{N+1}) r_{N+1}^{-1} \times B_j(r_{N+1}) a_{ijk}^\Gamma, \quad (3)$$

where $\bar{\Phi}_i$ are the channel functions while the splines $B_j(r)$ represent the continuum orbitals. The principal advantage of B splines is that they form an effectively complete basis, and hence no Buttke correction to the R matrix is needed in this case. The amplitudes of the wave functions at the boundary, which are required for the evaluation of the R matrix, correspond to the coefficient of the last spline, which is the only spline with nonzero value at the boundary.

The number of B splines and the R -matrix radius in the scattering calculations were chosen the same as in the calculation of the target bound states. We numerically calculated partial-wave contributions up to $L=35$ and, if necessary, used

a geometric extrapolation scheme to ensure the convergence of the partial-wave expansion. The cross-section calculations then were carried out in the same way as in the standard R -matrix calculations. Below we will show results from two different models, which we will label BSR49 and BSR23, respectively. The former couples the same 49 states as in our previous calculation [1], while BSR23 only includes the lowest 23 states in the close-coupling expansion. As seen from Table I of [1], these 23 states represent 11 spectroscopic bound states [up to $(4s6s)^1S$] and ten pseudostates with configurations $(3d^{10}4snl)$. All of these pseudostates still lie below the ionization threshold. Important additions in the BSR49 model are several states with a hole in the $3d$ shell, as well as a few low-lying $3d^{10}4skl$ states that simulate some couplings to the target ionization continuum just above threshold in the same way as done in the CCC approach.

IV. RESULTS AND DISCUSSION

In the present experiment we measured the photon count rate, which is proportional to the intensity of a spectral line of the radiation. This intensity arises from direct excitation of an atomic state, but usually also includes cascade radiation after the excitation of one or more higher-lying atomic levels. The signal may also be affected by an anisotropy in the photon emission as well as instrumental characteristics. When all instrumental properties and polarization are accounted for and only cascade contributions remain unresolved, the measured intensity is proportional to the emission cross section. Measurements of emission cross sections were discussed in detail by Heddle and Gallagher [28]. We carefully distinguish the excitation of a spectral line from the direct excitation of an atomic level, which is the primary excitation process considered theoretically, to determine an angle-integrated cross section. Photon excitation functions, measured previously in our laboratory during the study of negative-ion resonances (see, for example, [6,7]), usually are not corrected for any or all of these experimental factors.

The present measurements were performed over an energy mesh of 1 eV with an energy resolution of 0.250 eV. These values were adequate for the present study, but they are not fine enough to reproduce details in the cross section associated with negative-ion resonances or PCI effects associated with the decay of autoionizing states. These fine details, studied separately [6,7] before, are also relevant here and are indicated in the insets on the graphs. Also, the variation in the polarization of the decay photons due to negative-ion resonances, which is known to affect the light polarization P (see, for example, [4]), is not taken into account in the present corrections.

Experimental and theoretical results of the present study of excitation of the $(4s4p)^3P_1$, $(4s4p)^1P_1$, $(4s5s)^3S_1$, $(4s4d)^1D_2$, and $(4s4d)^3D_{1,2,3}$ states are presented below. The cross sections for excitation of singlet and triplet states are represented on linear and logarithmic scales, respectively, due to their very different energy dependence.

Theoretical results from four different models will be compared between themselves and experiment. As mentioned above, the CC29 and BSR23 models include only

negative-energy states in the close-coupling expansion. Agreement between the results from these two models would give the comforting indication that two independent theoretical formulations lead to similar results when the same physics is included in the model. Of course, some remaining discrepancies can be expected, especially if the results are sensitive to even small differences in the Zn target wave functions. Having established such a common base is important for comparison with the next two sets of much larger models: CCC206 and BSR49. As mentioned above, the CCC206 model accounts for significantly more ionization channels than BSR49, while the latter incorporates some effects from opening the $3d^{10}$ core.

A. Excitation of the $(4s4p)^1P_1$ state

The $(4s4p)^1P_1$ excited state of zinc decays by emission of 213.8 nm uv photons. The measured emission cross section for this line is shown in Fig. 1(a). The polarization of these uv photons could not be measured with our present polarimeter. Consequently the anisotropy in emission and its change with incident electron energy were corrected by using the theoretical CCC values for the light polarization P presented in Fig. 1(b). The experimental data in Fig. 1(a) were normalized to the theoretical emission cross section from the present CCC206 calculations, also shown in Fig. 1(a), at an energy of 40 eV.

The light polarization predicted by various theoretical models is shown in Fig. 1(b), in the CCC206 case for both the direct electron-impact excitation and the cascade-affected population of the $(4s4p)^1P_1$ state. The substantial variation in the light polarization makes a polarization correction essential to obtain the true energy dependence of this emission cross section. As expected in light of the large cross section value for this transition, compared to much smaller cross sections for excitation of higher-lying states, the predicted polarization is not influenced very much by cascades. Also, there is excellent agreement in the theoretical values calculated in the CCC206 and BSR49 models.

The excitation of the $(4s4p)^1P_1$ state is affected by the formation and the decay of temporary negative ions, which are formed above the ionization threshold and related to the excitation of an inner $3d$ electron. The inset in Fig. 1(a) shows a photon excitation function of the $(4s4p)^1P_1$ state with clear resonance structure; the details of which were given earlier [7]. This resonance structure is not revealed in the present emission cross sections due to the chosen experimental conditions. The BSR49 model contains a limited number of $3d$ -core excitation channels and indeed exhibits some variation in the cross section in the vicinity of the $3d^94s^24p$ autoionizing states. However, significantly more work seems to be required before agreement with experiment in the details may be expected.

The angle-ICSs for excitation of the $(4s4p)^1P_1$ state of zinc are presented in Fig. 1(c). We find very good agreement between the CC29 and BSR23 results for both the direct ICS and the emission cross section across the entire energy range. The CCC206 and BSR49 models agree well up to approximately 12 eV (the onset of $3d^94s^24p$ -core excited states)

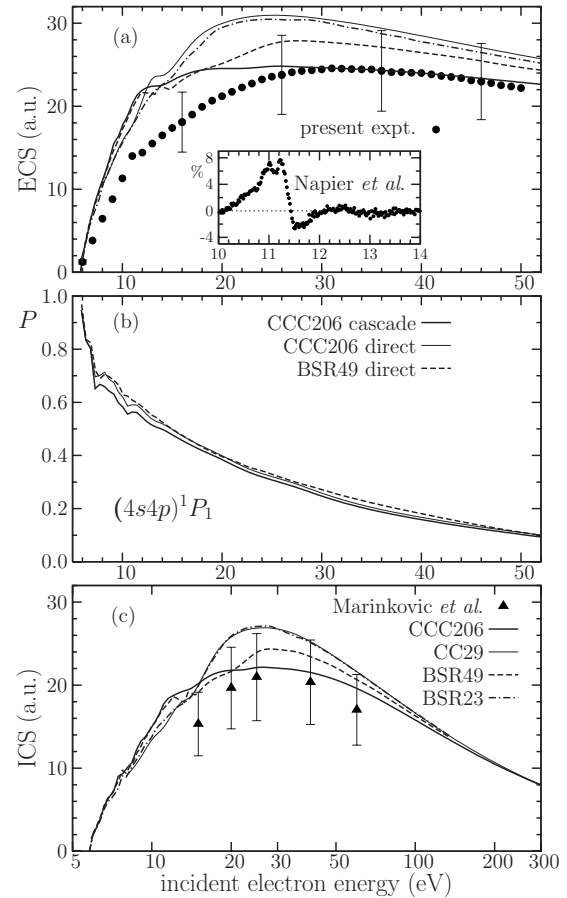


FIG. 1. Excitation of the $(4s4p)^1P_1$ state. (a) Emission cross section measured by observing 214 nm photons from the $(4s4p)^1P_1 \rightarrow (4s^2)^1S_0$ transition, normalized to the CCC emission cross section at 40 eV. The experimental data were corrected for the line polarization by using the CCC data for the apparent P . (b) Linear light polarization P from various theoretical models. (c) Angle-integrated cross sections for direct excitation. The theoretical CCC206, CC29, BSR49, and BSR23 calculations are described in the text. Also presented are ICS from Marinkovic *et al.* reported in Fursa *et al.* [2]. Inset (a): percentage of the resonance contribution (after subtraction of the background) in the high-resolution photon excitation function [7] (not resolved in the present measurements).

where the BSR49 results become somewhat lower. With increasing incident electron energy, coupling to the ionization continuum becomes relatively more important and thus the BSR49 model begins to overestimate both the direct and the emission cross sections. All theoretical models converge to the same high-energy limit, as would be expected due to the close agreement in the $(4s4p)^1P_1 \rightarrow (4s^2)^1S_0$ optical oscillator strength and excitation energy.

The present experimental emission cross sections agree well with the CCC206 results at energies of 25 eV and above. Below 25 eV, however, the experimental values lie consistently lower albeit within, or slightly above, the quoted uncertainties. The present emission cross section at 15 eV is consistent with the angle-integrated cross section measured by the Belgrade group [2] and the fact that cascades present a small contribution relative to the large value of this cross section. Both cross sections are somewhat lower at 15 eV

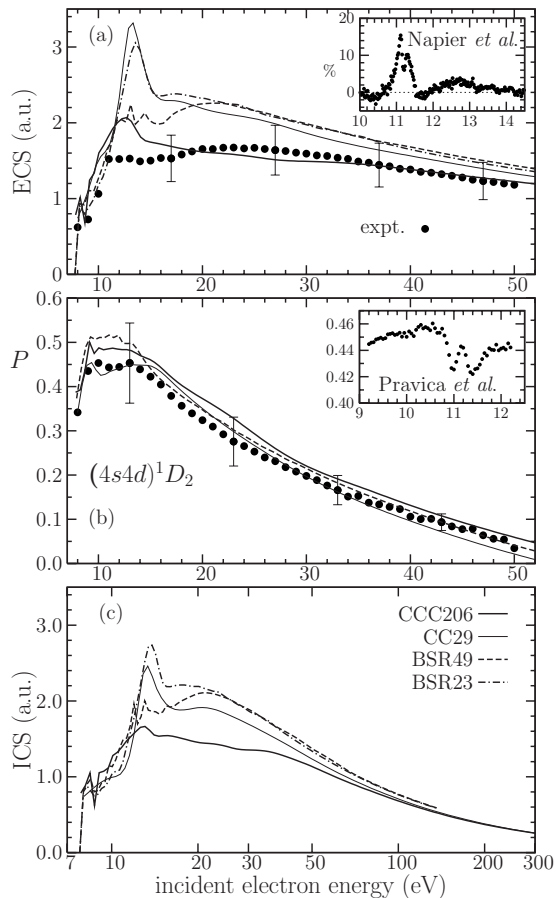


FIG. 2. Excitation of the $(4s4d) \ ^1D_2$ state. (a) Emission cross sections normalized at 40 eV to the CCC206 calculation. The measurements were carried out by detecting 636 nm photons from the $(4s4d) \ ^1D_2 \rightarrow (4s4p) \ ^1P_1$ transition, with a polarization correction applied. Inset (a): relative resonance contribution (after background subtraction) in the high-resolution photon excitation functions [7] (not resolved in present measurements). (b) Linear light polarization P . No error bars are shown since they are generally smaller than the size of the symbol. Inset (b): resonance structures in P as measured in [4]. (c) Angle-integrated cross section for direct excitation.

than the theoretical predictions, with the present value being slightly higher than that reported in [2] due to cascade contributions. Interestingly, the estimates of the direct ICS in [2] are also in good agreement with CCC206 results at all reported energies, except for the lowest point at 15 eV.

B. $(4s4d) \ ^1D_2$ state

The emission cross sections measured by detecting the 636 nm photons from the $(4s4d) \ ^1D_2 \rightarrow (4s4p) \ ^1P_1$ transition are shown in Fig. 2(a), together with results from the present CCC and BSR calculations. The inset in Fig. 2(a) shows again the percentage contribution of negative-ion resonances associated with excitation of one of the $3d$ electrons above the first ionization threshold. At higher energies, PCI effects are also possible [7]. Experimental and theoretical data for the light polarization P are shown in Fig. 2(b). The inset exhibits the fine structure due to negative-ion resonances ob-

served by Pravica *et al.* [4]. The theoretical ICS data are shown in Fig. 2(c). A comparison of previous theoretical predictions [1] and experimental observations of the resonance structure below the ionization threshold is discussed by Napier *et al.* [6].

Excitation of the $(4s4d) \ ^1D_2$ state is of special interest for several reasons. First, this optically forbidden transition with a transfer of two units of angular momentum and no fine structure is convenient for an experimental study, as the wavelength of the decay photons triggers almost the maximum response of our PMT. Furthermore, the isolated position of this line allows for the use of a filter with a wide transmission window and thus a high transmission. This permits the measurements to be performed and compared with theoretical predictions for a well-defined quantum state. On the other hand, describing an optically forbidden transition is generally more challenging for the theoretical approaches.

The present ECS data were normalized to the CCC206 results at 40 eV. A comparison of the CCC predictions and the experimental data reveals differences in both the absolute emission cross section values and the energy dependence of the cross sections at energies below about 20 eV, while good agreement is found at higher energies. From Figs. 2(a) and 2(c) we see that the energy dependence of the measured emission cross section is better reproduced by the BSR49 calculation, with a low-energy enhancement and a broad maximum centered around 20 eV. The difference in the absolute values between the BSR49 curve and experiment is a consequence of our choice of normalization and the fact that the results from the two models, CCC206 and BSR49, differ by more than the experimental uncertainties.

The theoretical results exhibit a strong dependence on the respective model. The CC29 and BSR23 calculations predict a very similar energy dependence of both the direct and the emission cross sections. Figures 2(a) and 2(c) show a large reduction in the ECS and ICS (with respect to the CC29 and BSR23 results) in the 11–15 eV region when coupling to ionization channels (CCC206 and $3d$ -core-excited channels in BSR49) is accounted for. The significant differences between the CCC206 and BSR49 results above 12 eV incident energy suggest a large effect of coupling to the ionization continuum. Note that the CCC and BSR results still differ at large incident electron energies (e.g., 100 eV). This is a manifestation of the remaining differences in the target wave functions used in these two methods.

In the narrow energy region above threshold where there are no cascade effects, the measured intensities are proportional to the angle-integrated cross sections. A comparison with earlier BSR calculations indicated a very good reproduction of the threshold behavior and the associated resonance structure [1,6].

At the energies above the ionization threshold where negative-ion resonances with a hole in the $3d$ subshell influence the emission cross section [see the inset of Fig. 2(a)], there is again a significant disagreement between the theoretical and experimental energy dependences. We note, however, that the BSR49 model, similar to the experiment, shows variations in the cross sections as a function of energy that are associated with excitation of a $3d$ electron. Nevertheless, the resonances and PCI effects in this energy region are still

not described adequately in the BSR49 model due to the complexity of the structures.

The light polarization P shown in Fig. 2(b) is essentially free of instrumental effects and could be measured with high statistical accuracy. The statistical uncertainties are generally smaller than the size of the symbol. For P , a relative parameter determined by the ratio of transmitted intensities, the agreement between experiment and theory is better than for the cross sections at energies above approximately 16 eV. Somewhat larger differences are observed in the near-threshold region and just above the ionization threshold, where excitation of a $3d$ electron has an indirect influence on the cross section.

Measurements of all three Stokes polarization parameters, the spin-independent linear polarization P (often denoted P_1 in this context) as well as the linear polarization P_2 and the circular polarization P_3 , both of which can only be different from zero for an incident spin-polarized electron beam [11], indicate the importance of exchange and spin-orbit effects when the excitation also proceeds via negative-ion resonances [4]. This structure is not predicted by any of the current theories, thereby indicating that a sophisticated inclusion of relativistic effects as well as electron correlation for the excited $3d$ -orbital configuration will be essential. Resonance effects on the spin-independent polarization parameter P are shown in the inset of Fig. 2(b).

C. Excitation of the $(4s4p)^3P_1$ state

The $(4s4p)^3P_{0,2}$ states are metastable against decay to the only lower (ground) state, being forbidden by the $\Delta S=0$ spin selection rule. Due to an intermediate-coupling 1P_1 admixture, however, the $(4s4p)^3P_1 \rightarrow (4s^2)^1S_0$ transition at a wavelength of $\lambda=307.6$ nm can be observed as a weak intercombination line. The emission cross section for the $(4s4p)^3P_1$ state measured from the excitation threshold to 50 eV incident energy is depicted in Fig. 3(a). The measured signal was again normalized to the CCC value for the emission cross section at 30 eV. Due to the long lifetime (30 μ s) of the $(4s4p)^3P_1$ state [29] and a residual magnetic field of approximately 5 mG in the interaction region, the emitted radiation is practically depolarized through the Hanle effect, and thus no polarization correction is needed for the measured intensities.

Note that the nonrelativistic CCC and BSR cross sections are obtained as the sum of all three fine-structure components. Consequently, only one third (the statistical weight) of the results calculated for the $(4s^2)^1S \rightarrow (4s4p)^3P$ transition is displayed in Fig. 3(a) for the emission cross section and in Fig. 3(b) for the direct excitation cross section. The singlet admixture mentioned above is so small for this state that it was neglected in the calculation of the cross sections. We see very good agreement between the CC29 and BSR23 results over the entire energy range. Above the ionization threshold, however, these two models overestimate the cross section when compared to the CCC206 and BSR49 predictions. The agreement between CCC206 and BSR49 holds to about 15 eV. At higher incident electron energies the BSR49 results go above CCC206, which is almost certainly due to the incom-

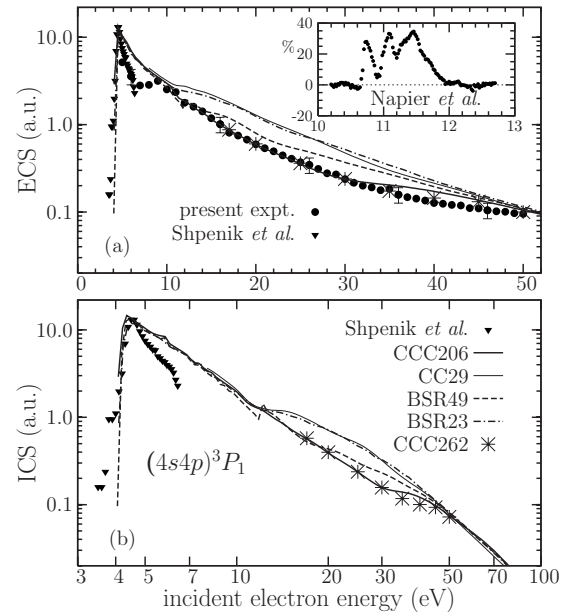


FIG. 3. Excitation of the $(4s4p)^3P_1$ state. (a) Emission cross sections derived from observing the 307.6 nm photons from the $(4s4p)^3P_1 \rightarrow (4s^2)^1S_0$ transition. Inset: relative resonance contribution measured by Napier *et al.* [7] not resolved in the present measurements. (b) Angle-integrated cross sections. The present experimental data were normalized to the CCC emission cross section at 30 eV. The ICS measurements of Shpenik *et al.* [18] (see text for normalization) are also shown.

plete account of coupling to the ionization channels in the former model.

The angle-integrated cross sections from the two models are shown in Fig. 3(b). The energy scale in this panel was extended to 100 eV in order to demonstrate the convergence of all theoretical predictions toward each other at high energies. The calculations exhibit the same features for the direct excitation cross section as for the emission cross section: (1) there is very good agreement between all theoretical results below the ionization threshold and (2) the CCC206 results are significantly lower than those from all the other models in the intermediate-energy region due to the importance of coupling to the ionization channels. In fact, for this state adding even more states in the CCC262 model further lowers the theoretical values in the energy region between 30 and 50 eV and removes the small shoulder seen in the CCC206 results. Note that the jump in the BSR49 results near 11 eV is due to the opening of the $3d^{10}$ core.

The present experiment, when normalized to the CCC206 results at 30 eV, shows good agreement with theory at all energies above approximately 10 eV. Much lower than predicted values, however, were measured at energies down to threshold. The only other cross-section measurement for this state, carried out by Shpenik *et al.* [18], supports the present observation of lower near-threshold values than predicted by any of our theories. These measurements were performed by detecting the scattered electrons in an energy region where the present photon detection is free of cascades and, therefore, the two data sets are directly comparable. They are included in both panels of Fig. 3. The cross sections reported

by Shpenik *et al.* [18] correspond to the sum of the three unresolved fine-structure components and were renormalized at the near-threshold peak to the CCC206 values for $J=1$. Therefore, only the energy dependence, which shows a fast decrease in the threshold peak with increasing projectile energy, is relevant for comparison. Clearly, the shoulder structure observed in our experiment for incident energies between 6 and 10 eV is not reproduced by any of our theories.

The structures observed in the present emission cross section at low energies are once again associated with negative-ion resonances. They were observed both below [6] and above [7] the ionization threshold at 9.394 eV. These structures are not seen clearly in the present data, as they are too narrow compared to the present energy mesh and resolution. Below the ionization threshold they cause variations of up to 10% in the total detected intensity. Above the ionization threshold and in the region of the $3d^9 4s^2 4p$ autoionizing states, the situation is different. Several broad negative-ion resonances with dominant electron configuration $3d^9 4s^2 4p^2$ cause variations of around 30%, as shown in the inset of Fig. 3(a). Our earlier work exhibits the details of this photon excitation function [7]. The theoretical approaches used in the present study either do not account for the opening of the $3d$ subshell at all (CCC) or still not in a sufficient way (BSR) to achieve convergence. Hence they are not expected to reproduce the resonance features in this autoionizing region.

D. $(4s4d)^3D_{1,2,3}$ states

Excitation of the $(4s4d)^3D_{1,2,3}$ states was studied by observing all lines arising from the decay to the various fine-structure components of the $(4s4p)^3P_{0,1,2}$ multiplet. These consist of six lines with wavelengths between 328.2 and 334.6 nm. All of these lines were detected but with different efficiencies due to variations in the transmission of the interference filter centered around 334.2 nm. Consequently, the emission detected does not accurately present the sum of all fine-structure lines and comparison with theory is somewhat problematic. In light of this immediate uncertainty, no polarization correction of the emitted radiation was applied. We note, however, that such a correction for this particular multiplet of lines is not expected to be significant because of a strong fine-structure depolarization.

The present ECS measurements, Fig. 4), were again normalized to the CCC206 results at 30 eV. All theories predict a large cascade contribution (up to 40%) to the $(4s4d)^3D_{1,2,3}$ ECS. There is a good agreement in the energy dependence of the measured and the theoretical ECS in the interval from 25 to 50 eV, while significant discrepancies are found at lower energies, particularly at the cross-section maximum around 11 eV. Again the influence of negative-ion resonances, and for this state PCI effects as well, has not been accounted for in the theories. Although this omission might explain part of the observed differences, this problem needs further attention.

All the theoretical results agree well with each other below the ionization threshold. The CC29 and BSR23 models are in good agreement over the entire energy range. The CCC206 and BSR49 models predict similar ECS and ICS

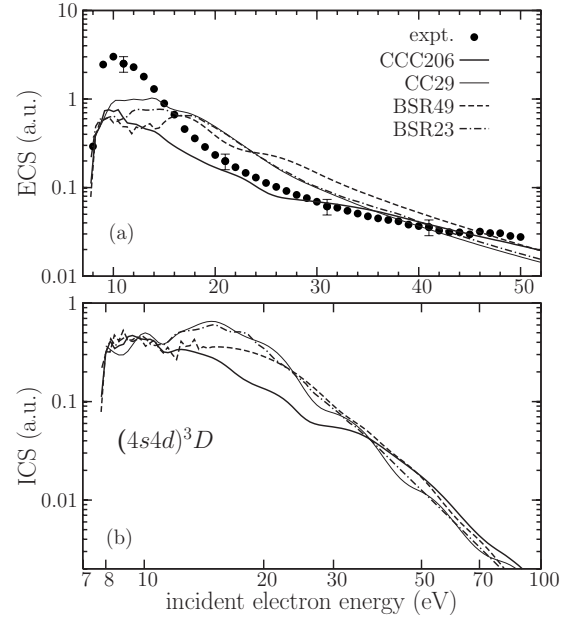


FIG. 4. Excitation of the $(4s4d)^3D_{1,2,3}$ states. (a) Emission cross section derived from observing 328–335 nm photons from the $(4s4d)^3D_{1,2,3} \rightarrow (4s4p)^3P_{0,1,2}$ transitions, normalized to the CCC206 emission cross section at 30 eV. All components of the transition were detected, although with different efficiencies (see text). The line polarization was not measured for this state, and no polarization correction was applied. (b) Angle-integrated cross section.

values up to 12 eV. The CCC206 results are lower than those from the other theories in the 12–40 eV region, thus indicating that coupling to the ionization channels is likely to play a significant role at these energies. This is not surprising, given that this transition is both spin and angular-momentum forbidden.

E. $(4s5s)^3S_1$ state

The $(4s5s)^3S_1$ state can decay to all three fine-structure levels of the $(4s4p)^3P_{0,1,2}$ multiplet. We observed the transition to the $J=1$ of the lower state at $\lambda=481$ nm, which was well resolved from the other two fine-structure components. Experimental and theoretical data for this excitation are presented in Figs. 5(a) and 5(b).

The theoretical results reveal good agreement between the CCC206 and BSR49 calculations from the excitation threshold to 12 eV for the ECS shown in Fig. 5(a). At intermediate incident electron energies, the BSR49 cross sections are larger than those from CCC206. This is again consistent with the incomplete account of coupling to the ionization channels in the BSR49 model. The CC29 and BSR23 calculations agree well over the entire energy regime. Not surprisingly, they both significantly overestimate the ECS above the ionization threshold.

The experimental emission cross section shown in Fig. 5(a) was not corrected for polarization effects. The latter correction is expected to be small, as all light polarization for this line arises from cascade population. Our preliminary

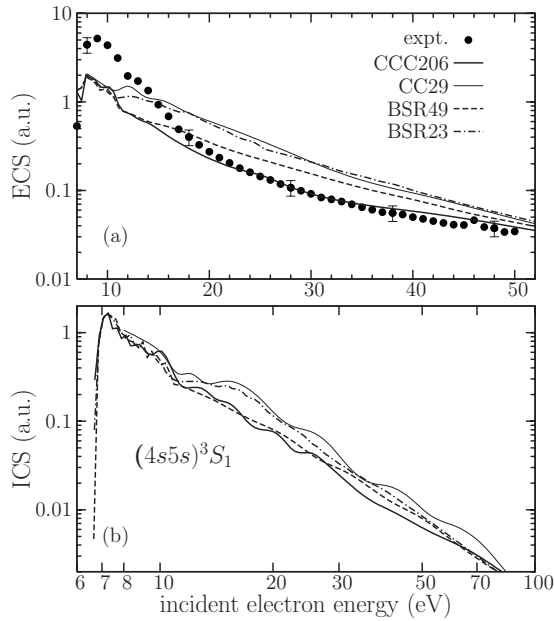


FIG. 5. Excitation of the $(4s5s) \ ^3S_1$ state. (a) Emission cross sections derived from observing 481 nm photons from the $(4s5s) \ ^3S_1 \rightarrow (4s4p) \ ^3P_1$ transition. (b) Angle-integrated cross sections.

measurements with a spin-polarized electron beam show that the spin-independent polarization parameter P is essentially zero for incident energies up to approximately 1 eV above the threshold and then exhibits a steplike rise to $\approx 6\%$ due to the onset of cascades.

A strong influence of negative-ion resonances is predicted for excitation of the $(4s5s) \ ^3S_1$ state in the near-threshold energy region by both previous BSR [1] and the present CCC206 calculations. These findings agree with our preliminary observations in high-resolution photon excitation functions, where significant structures due to negative-ion resonances, both below and above the ionization threshold, are observed [30]

As a number of higher-lying triplet states populate the $(4s5s) \ ^3S_1$ state via cascades and some of them decay entirely via this state, cascade effects are found to be a dominant source of this radiation, contributing more than 60% to the ECS above 9 eV. Some of the resonance effects can be observed via cascades. Similarly, structures due to PCI that are observed to yield, for example, a substantial contribution to the excitation of the $n=4,5,6 \ ^3D_{1,2,3}$ states [7], are expected to also be present in the excitation functions of the $(4s5s) \ ^3S_1$ state. Consequently, the calibration was performed at 30 eV, where population of this level is likely not affected by either resonances or PCI effects.

The experimental emission cross sections shown in Fig. 5(a) agree well with the CCC206 results at incident energies above approximately 20 eV. At lower energies, they are progressively higher than calculated, with a significantly (about a factor of 5) higher value in the cross-section maximum around 11 eV. All theories agree well with each other at these low energies, but they are not accounting well for the influence of either negative-ion resonances or PCI effects in the autoionizing region of zinc. Nevertheless, the observed dif-

ferences seem too large to be explained solely by the latter shortcomings of the theories.

V. CONCLUSIONS

The present study has established e -Zn excitation cross sections for five states which include optically allowed $(4s4p) \ ^1P_1$, symmetry-forbidden $(4s4d) \ ^1D_2$, spin-forbidden $(4s4p) \ ^3P_1$, or both symmetry- and spin-forbidden $(4s5s) \ ^3S_1$ and $(4s4d) \ ^3D_{1,2,3}$ transitions. The experimental data were compared with predictions from two independent state-of-the-art theoretical models, namely, CCC and BSR, to assess the importance of coupling to the ionization continuum and opening of the $3d$ -core subshell. Comparing the experimental angle-integrated emission and direct excitation cross sections [2,18] and the results from the CCC and BSR methods, obtained with a varying number of states included in the respective close-coupling expansions, leads to a number of conclusions.

First, the CCC and BSR methods produce very similar cross-section results when a similar close-coupling expansion is utilized. This was demonstrated by comparing predictions from the CC29 and BSR23 models; both of which include only negative-energy (bound) target states. Having established this common ground, we proceeded to investigate the importance, or lack thereof, of coupling to various ionization channels. These included both ionization of the outer shell $4s$ electron and promotion of an inner $3d$ -core electron to produce an autoionizing state. Compared to the CC29 results, we observed a significant reduction in the calculated cross sections in the CCC206 model (which includes single ionization from the $4s$ subshell) for all transitions considered in this work in the intermediate-energy regime. Comparison of the CCC206 and BSR49 results showed close agreement up to approximately 13 eV incident energy for most of the cross sections presented here. Since an essential difference between the two models is the partial accounting of $3d^9 4s^2 kl$ -core-excited states in the BSR49 approach, we suspect that the latter states only affect the valence-shell transitions for incident electron energies in the vicinity of their respective thresholds.

Furthermore, the comparison of the theoretical and experimental ECS values reveals some systematic patterns. Clearly, most of the differences are observed at low impact energies, typically below 20–25 eV. Note, however, that the deviations vary substantially for the individual excited states. For the singlet states investigated here, $(4s4p) \ ^1P_1$ and $(4s4d) \ ^1D_2$, the experimental ECSs are lower at small energies, while they are considerably higher for two of the triplet states, namely, $(4s4d) \ ^3D_{1,2,3}$ and $(4s5s) \ ^3S_1$. Excitation of the $(4s4p) \ ^3P_1$ state, on the other hand, is a somewhat peculiar case. The energy dependence in the high-energy regime is well reproduced by the CCC approach, as well as the other theories. However, since coupling to the ionization continuum is expected to be important for this spin-forbidden transition, normalization to the CCC206 value at 30 eV seems most reasonable. Recall that none of our theories reproduces the rapid decrease in the ECS between the maximum and about 6 eV, followed by a shoulder that extends to incident energies of about 10 eV.

At the present time, we are unable to explain the magnitude of these differences. We do not believe, however, that the large discrepancies between experiment and theory are due to instrumental effects, such as an inadequate treatment and variation of the beam transmission or the focusing of the electron beam at lower energies. For the singlet states, $(4s4p) ^1P_1$ and $(4s4d) ^1D_2$, the differences observed at low impact energies still yield reasonable agreement with theory, comparable in magnitude to the differences between the angle-integrated cross sections from the two presumably best models, CCC206 and BSR49. Nevertheless, the energy dependence of the observed emission cross section around the cross-section maximum is definitely in disagreement with that predicted in all our calculations.

The much larger differences between the experimental and theoretical cross-section values for the three triplet states, $(4s4p) ^3P_1$, $(4s4d) ^3D_{1,2,3}$, and $(4s5s) ^3S_1$, are even more puzzling. Interestingly, the region of 10–15 eV, where we observed the largest discrepancies, is also the regime where large structures were reported in the optical excitation functions by Napier *et al.* [7]. Two different effects, negative-ion resonances and postcollision interaction, both associated with promotion of one of the $3d$ electrons and governed by strong electron correlations, were found to affect significantly the excitation cross sections. While some initial steps are taken in the BSR49 approach, neither effect is currently accounted for to sufficient accuracy in any of our theoretical models.

These experimental observations, combined with the relatively large cross sections for excitation of the $3d^94s^24p$ autoionizing states as evidenced by energy-loss spectra [5,31], point to some possible explanations and future directions for theory. The coupling between the $3d^94s^2nl$ and $3d^{10}4sn'l'$ manifolds, together with an expected strong singlet-triplet mixing, might lead to significant enhancements of the exci-

tation cross sections for triplet states and correspondingly to reductions in the singlet excitation cross sections. Such a trend would be needed to reduce the observed discrepancies between the present experimental data and the theoretical predictions. Theoretical methods that account for relativistic effects either fully (based on the Dirac formalism) or approximately (based on the Breit-Pauli approach) are required apparently for this problem in order to shed more light on the potential origin of these discrepancies. While we are working in this direction, we emphasize that the calculations reported in this paper are at the limit of what can be done at the present time. It will likely take years before these calculations can be improved substantially.

Finally, the present study is intended to serve as a basis for future extensions to even more complex scattering processes involving inner $3d$ electrons. Such events are likely governed by strong electron correlations as well as relativistic effects. For theory, such extensions present a very difficult task. Meeting the challenges will require code and algorithm development, including versions of the present computer codes that are suitable for massively parallel supercomputing platforms. Experimentally, electron-impact excitation studies in these systems will open a wide field of investigating in great detail the effects of electron correlation and the role of angular momenta in complex transition metals.

ACKNOWLEDGMENTS

This work was supported by the Australian Research Council, Curtin University, and the University of Western Australia. O.Z. and K.B. are supported by the United States National Science Foundation under Grant Nos. PHY-0555226 and PHY-0775575. We are grateful for access to the Australian National Computational Infrastructure and its Western Australian node iVEC.

-
- [1] O. Zatsarinny and K. Bartschat, *Phys. Rev. A* **71**, 022716 (2005).
- [2] D. V. Fursa, I. Bray, R. Panajotović, D. Šević, V. Pejčev, D. M. Filipović, and B. P. Marinković, *Phys. Rev. A* **72**, 012706 (2005).
- [3] L. Pravica, J. F. Williams, D. Cvejanovic, and S. A. Napier, *Phys. Rev. A* **75**, 012721 (2007).
- [4] L. Pravica, D. Cvejanovic, J. F. Williams, and S. A. Napier, *Phys. Rev. A* **75**, 030701(R) (2007).
- [5] S. Napier, D. Cvejanovic, J. F. Williams, and L. Pravica, *J. Phys. B* **40**, 1323 (2007).
- [6] S. A. Napier, D. Cvejanovic, J. F. Williams, and L. Pravica, *Phys. Rev. A* **78**, 022702 (2008).
- [7] S. A. Napier, D. Cvejanovic, J. F. Williams, and L. Pravica, *Phys. Rev. A* **78**, 032706 (2008).
- [8] M. Born, *J. Phys. D* **34**, 909 (2001).
- [9] N. Andersen and K. Bartschat, *J. Phys. B* **35**, 4507 (2002).
- [10] N. Andersen and K. Bartschat, *Polarization, Alignment and Orientation in Atomic Collisions* (Springer-Verlag, New York, 2001).
- [11] K. Bartschat and K. Blum, *Z. Phys. A* **304**, 85 (1982).
- [12] N. Andersen, K. Bartschat, J. T. Broad, and I. V. Hertel, *Phys. Rep.* **279**, 251 (1997).
- [13] I. Bray, D. V. Fursa, A. S. Kheifets, and A. T. Stelbovics, *J. Phys. B* **35**, R117 (2002).
- [14] K. Bartschat, *Complete Scattering Experiments*, edited by U. Becker and A. Crowe (Kluwer Academic/Plenum, New York, 2001), Chap. 2.
- [15] X. Guo, D. F. Mathews, G. Mikaelian, M. A. Khakoo, A. Crowe, I. Kanik, S. Trajmar, V. Zeman, K. Bartschat, and C. J. Fontes, *J. Phys. B* **33**, 1895 (2000).
- [16] R. Panajotović, D. Šević, V. Pejčev, D. M. Filipović, and B. Marinković, *Int. J. Mass Spectrom.* **233**, 253 (2004).
- [17] W. Williams and D. Bozinis, *Phys. Rev. A* **12**, 57 (1975).
- [18] O. B. Shpenik, I. V. Chernishova, and J. E. Kontros, *Radiat. Phys. Chem.* **68**, 277 (2003).
- [19] D. V. Fursa and I. Bray, *Phys. Rev. Lett.* **100**, 113201 (2008).
- [20] O. Zatsarinny, *Comput. Phys. Commun.* **174**, 273 (2006).
- [21] O. Zatsarinny and K. Bartschat, *Phys. Rev. A* **77**, 062701 (2008).

- [22] O. Zatsarinny, K. Bartschat, M. Maslov, M. J. Brunger, and P. J. O. Teubner, *Phys. Rev. A* **78**, 042713 (2008).
- [23] J. E. Furst, D. H. Yu, P. A. Hayes, C. M. D'Souza, and J. F. Williams, *Rev. Sci. Instrum.* **67**, 3813 (1996).
- [24] I. C. Percival and M. J. Seaton, *Philos. Trans. R. Soc. London, Ser. A* **251**, 113 (1958).
- [25] D. V. Fursa and I. Bray, *Phys. Rev. A* **52**, 1279 (1995).
- [26] D. V. Fursa and I. Bray, *J. Phys. B* **30**, 757 (1997).
- [27] O. Zatsarinny and C. F. Fischer, *J. Phys. B* **35**, 4669 (2002).
- [28] D. W. C. Heddle and J. W. Gallagher, *Rev. Mod. Phys.* **61**, 221 (1989).
- [29] F. W. Byron, M. N. McDermott, R. Novic, B. W. Perry, and E. B. Saloman, *Phys. Rev.* **134**, A47 (1964).
- [30] S. A. Napier, D. Cvejanovic, J. F. Williams, and L. Pravica, *J. Phys.: Conf. Ser.* (to be published).
- [31] S. A. Napier, D. Cvejanovic, J. F. Williams, and L. Pravica, S. N. Samarin, A. D. Seargeant, P. Guagliardo, and P. Wilkie (unpublished).